Performance Evaluation of Wavelet-Coded OFDM on a 4.9 Gbps W-Band Radio-over-Fiber Link

Cavalcante, Lucas Costa Pereira; Rommel, Simon; Dinis, Rui; Junior, L. G. Q. Silveira; Silveira, Luiz F. Q. ; Tafur Monroy, Idelfonso

Published in:
Journal of Lightwave Technology

Link to article, DOI:
10.1109/JLT.2017.2701358

Publication date:
2017

Document Version
Peer reviewed version

Performance Evaluation of Wavelet-Coded OFDM on a 4.9 Gbps W-Band Radio-over-Fiber Link

Lucas C. P. Cavalcante, Simon Rommel, *Student Member, IEEE*, Rui Dinis, *Senior Member, IEEE*, L. G. Q. Silveira Junior, *Member, IEEE*, L. F. Q. Silveira, *Member, IEEE*, and Idelfonso Tafur Monroy, *Senior Member, IEEE*

***Abstract*—Future generation mobile communications running on mm-wave frequencies will require great robustness against frequency selective channels. In this work we evaluate the transmission performance of 4.9 Gbps Wavelet-Coded OFDM signals on a 10 km fiber plus 58 m wireless Radio-over-Fiber link using a mm-wave radio frequency carrier. The results show that a 2×128 Wavelet-Coded OFDM system achieves a bit-error rate of 1e-4 with nearly 2.5 dB less signal-to-noise ratio than a convolutional coded OFDM system with equivalent spectral efficiency for 8 GHz-wide signals with 512 sub-carriers on a carrier frequency of 86 GHz. Our findings confirm the Tzannes' theory that wavelet coding enables high diversity gains with a low complexity receiver and, most notably, without compromising the system's spectral efficiency.**

***Index Terms*—Wavelet-Coding, OFDM, Radio-over-Fiber, W-Band, mm-Wave, Frequency Selectivity.**

I. Introduction

AS THE fifth generation (5G) of mobile communications technology is developed and implemented, worldwide solutions propose the use of much greater spectrum allocations in both licensed and unlicensed spectrum, including the mm-wave frequency band [1]–[5]. Radio-over-fiber links allow straight forward integration of the mobile front- and backhaul with deployed optical distribution networks, while readily offering the use of large modulation bandwidths [1], [2], [5]. Such a requirement imposes a critical demand for broadband wireless links, implying in high-bit-rate transmissions that are loudly subjected to channel-induced inter-symbol interference (ISI) incurred by frequency selectivity [6].

Adding frequency diversity in an Orthogonal Frequency Division Multiplexing (OFDM) design is an effective way of mitigating the effect of frequency-selective fading, which is generally achieved by sub-carrier redundancy, or channel coding [7]. Therefore, most of the practical OFDM systems are associated with forward error correction (FEC) codes [8] such as Reed-Solomon (RS) code [9], [10], convolutional code [11], [12], trellis-coded modulation (TCM) [13], turbo code [14], and low-density parity-check (LDPC) code [15].

The Wavelet-Coding scheme has been proposed in [16] as a new diversity strategy that: i) does not add redundancy to the original bit stream, which makes it a very competitive solution in comparison to other coding schemes such as convolutional or LDPC codes [7]; that ii) has a considerable simplified receptor, beating trellis or turbo based decoders in terms of computational costs [7]; and that iii) shows enormous performance gains on fading channels, as demonstrated over the past years [17], [18].

Recently, in [19], the Wavelet-Coding was used to enable high time-diversity gains in Doppler-rich channels with no cost to system spectral efficiency and yet with very simple decoding. Those findings were extended in [20], where it has been found that the Wavelet-Code can substantially compensate for the combined effects of deep frequency fading and error bursts that disrupt orthogonality among OFDM sub-carriers.

In this work, we experimentally demonstrate the transmission of 4.9 Gbps Wavelet-Coded (WC) OFDM signals as proposed in [20] on a 10 km fiber plus 58 m wireless Radio-over-Fiber link using a mm-wave carrier frequency of 86 GHz. We evaluate the performance of 2×128 and 2×8 WC-OFDM schemes in terms of bit-error rate (BER) for several OFDM resolutions. The results are contrasted with an uncoded scheme and a state-of-the-art coded scheme, all of them with equivalent spectral efficiency of 1 bit/s/Hz.

Our findings show that the proposed system substantially compensates for the effects of frequency distortion caused by electronic and optical components with non-flat frequency response. The results confirm the theory of Tzannes [16] that WC enables high diversity gains with a low complexity receiver, and, most notably, without compromising the system's spectral efficiency. The results also validate the solution proposed in [17] on modulation schemes that support the integration of WC with power-limited systems. To the best of the authors' knowledge, the transmission of WC signals has never been experimentally demonstrated.

The proposed system fits as a key enabler for the use of mm-wave frequencies in future generation mobile communications for outdoor medium distance links such as (a) building-to-building communication, (b) recovery and protection of fiber links, (c) mobile front-/backhaul, (d) spanning obstacles for providing broadband access to rural ares, and (e) short-range indoor wireless distribution. The network scenario for the

Manuscript received March 10, 2017; revised ??; accepted ??.

L. Cavalcante thanks CAPES for support under scholarship number 11964-13-8. R. Dinis thanks FCT-MCES and IT for suppurt under project UID/EEA/50008/2013. This work was partly funded by the DFF FTP mmW-SPRAWL project and the EC FP7-ICT IPHOBAC-NG project under grant No. 619870.

Lucas C. P. Cavalcante, Simon. Rommel, and Idelfonso Tafur Monroy are with the Department of Photonics Engineering, Technical University of Denmark, DK-2800 Kgs. Lyngby, Denmark. e-mail: luca@fotonik.dtu.dk.

Rui Dinis is with the Instituto de Telecomunicações and DEE-FCT, Universidade Nova de Lisboa, Caparica, 2829-516 Lisboa, Portugal.

L. G. Q. Silveira Junior and L. F. Q. Silveira are with the Departamento de Engenharia de Computação, Universidade Federal do Rio Grande do Norte, Mirassol, 59072-970 Natal, Brazil.

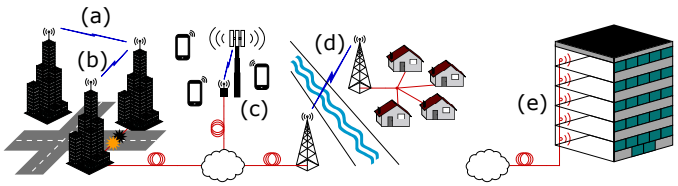

Fig. 1. Network scenarios for the hybrid fiber-wireless link.

hybrid fiber-wireless link proposed in this work is represented in Fig. 1.

This paper is organized as follows: Section II explains the wavelet coding / decoding algorithm; Section III describes the proposed system in detail, including transmission and reception schemes, and the experimental setup. Section IV explains the applied methodology and discusses the results. Finally, Section V draws the conclusions.

II. Wavelet-Coding Scheme

Wavelet-Coding enables diversity gains without necessarily diminishing the system's efficiency [16] through the use of Wavelet-Coefficient Matrices (WCMs). WCMs have arbitrarily long rows, which are orthogonal to each other, even when moved and/or added. This work focuses on the use of integer flat WCMs. The matrix $A = (a_k^j)$ with dimensions $m \times mg$, whose coefficients a_k^j take value in the integer set $\{+1, -1\}$ is said to be a wavelet matrix with rank m and genus g if it satisfies the *modified wavelet scaling conditions* [16], [21]. Those conditions ensure that:

i) the sum of the elements in the first row of A is equal to the matrix rank m; that
ii) the sum of the elements from all remaining rows of A is equal to zero; and that
iii) the WCM's rows are mutually orthogonal, even when shifted by m-multiple positions, and orthogonal to copies of themselves shifted by m-multiple positions.

The diversity gains from WC can be continuously enhanced by employing WCM with larger dimensions [17].

A. Coding Algorithm

In this approach, the wavelet encoder multiplies successive source bits by distinct rows of a WCM, called wavelet codewords, to encode the information bits. Let a discrete source generate statistically independent and identically distributed (i.i.d.) bits $\{x_n\} \in \{+1, -1\}$. The wavelet symbol produced at time $n = pm + q$ is expressed by

$$y_{pm+q} = \sum_{j=0}^{m-1} \sum_{l=0}^{g-1} a_{lm+g}^{j} x_{(p-l)m+j}. \quad (1)$$

The produced wavelet symbols take values in the set $\{-mg, -mg+2, \ldots, 0, \ldots, mg-2, mg\}$ with probability

$$Pr(y_n = 2k - mg) = \binom{mg}{k} 0.5^{mg}, 0 \leq k \leq mg. \quad (2)$$

Within this process, the information represented by an information bit is spread along the transmitted sequence, causing a small part of the signal to contain information about an entire block of data. This way, it is expected that the coded signal can withstand nullifying of closely-spaced symbols. This process can be used for improving robustness against the combined effects of varying fading and noise bursts [18], [19]. The longer the matrices employed, the larger the bit-blocks that will be coded by each row, and therefore more frequent deep fading of the channel may occur without disrupting the transmission. It can be verified that m information bits are encoded in m wavelet symbols sent during m signaling intervals, thus allowing a spectral efficiency of 1 bit/s/Hz.

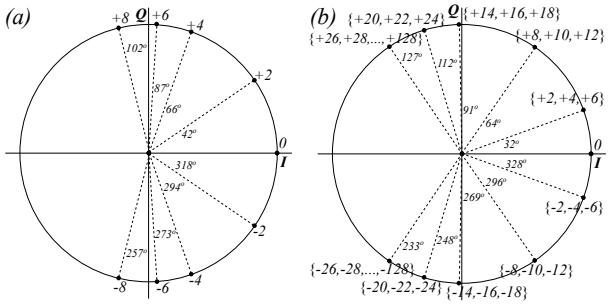

Fig. 2. PSK constellations after mapping of wavelet symbols. *(a)* 9-PSK constellation for 2×8 wavelet coding; *(b)* 11-PSK constellation for 2×129 wavelet coding.

In this work, wavelet matrices with parameters $m_1 = 2$, $g_1 = 4$, and $m_2 = 2$, $g_2 = 64$ are employed, therefore with dimensions $\mathcal{D}_1 = 2 \times 8$ and $\mathcal{D}_2 = 2 \times 128$, meaning that the wavelet decoder at the receiver must decide between 9 levels for the case $\mathcal{D}_1$ and 129 levels for the case $\mathcal{D}_2$.

In [17], a solution has been proposed for integrating wavelet-coding with power-limited systems, resulting in probabilistically shaped, non-uniform constellation diagrams that take into account the facts that:

i) for an i.i.d. source, successive wavelet symbols have similar levels;
ii) the generated wavelet levels are not equiprobable, according to Eq. (2), and consequently the performance gains of these systems are significantly influenced by their modulation scheme;
iii) decision errors between two close wavelet levels do not necessarily result in any bit errors, whereas decision errors between wavelet levels far from each other may considerably degrade correct bit estimation.

Based on that solution, the transmitted data symbols for the case $\mathcal{D}_1$ will belong to a 9-PSK (i.e. phase shift keying) signal space according to Fig. 2(a). In order to avoid performance degradation due to constellation crowding on the case $\mathcal{D}_2$, a many-to-one mapping $\mathcal{P}(\cdot)$ of the wavelet symbols generated by Eq. (1) is performed onto an 11-PSK signal space, according to Fig. 2(b). The effect of such a quantization mapping on the BER floor is reported in [17].

B. Decoding Algorithm

At the receptor, the transmitted information bit sequence $\{x_n\}$ at the moment $i = m(g + p) - 1$ can be estimated from the wavelet symbol sequence y_n by using a bank of

m correlators of length mg matched with the m rows of the WCM as

$$z_i^j = \sum_{k=0}^{mg-1} a^j_{(mg-1)-k}(y_{i-k} + e_{i-k}), \quad (3)$$

where e_{i-k} is an integer random variable that denotes the *demodulation noise* [18]. Due to the orthogonally of the MCWs' rows, the original transmitted bits can be estimated as $\hat{x}_{j+1-(mg-1)} = sgn(z_i^j)$. The decoding process' computational simplicity is one of the main features of wavelet coding [16], [21].

III. System Description

Fig. 3 shows the block diagram of the proposed transmission system together with the actual laboratory setup in terms of three main parts: A) Digital transmitter (top-left); B) experimental setup (top-right); and C) digital receiver (bottom), as described in the following subsections.

A. Digital Transmitter

A pseudo-random sequence of bits x with length l is generated and coded according to section II-A. The wavelet symbols resulting from Eq. (1) are randomly interleaved and delivered to an inverse fast Fourier transform (IFFT) after serial-to-parallel conversion in order to form OFDM symbols, expressed in time domain as [22]:

$$s[n] = \mathcal{F}^{-1}(S[k]), \quad k = 0, 1, \ldots, N-1, \quad (4)$$

where $\mathcal{F}(\cdot)^{-1}$ denotes the inverse Fourier transform operation with size N, and $S[k]$ is the frequency-domain symbol for the k-th sub-carrier.

OFDM symbols with $N = 512$, $N = 1024$, and $N = 2048$ sub-carriers are considered in this work. For each OFDM symbol, the transmitted symbols are denoted as $\mathbf{S} = [S[0], S[1], \ldots, S[N-1]]^T$, where the first N_{null} tones and the last N_{null} tones are designated as null sub-carriers to be used as guard bands. The number of required sub-carriers is a composite of the $l + m * g - 2$ coded output symbols plus null sub-carriers. The IFFT sizes are chosen to be fixed, always equal to such a number of required sub-carriers.

Every OFDM symbol has pilot tones $\mathbf{P}$ at periodically-located sub-carriers, which are used for a frequency-domain interpolation to estimate the channel response along the frequency axis at the receptor. Let S_f be the period of the pilot tones in frequency domain to be allocated along the N_U used sub-carriers, then the pilot tones $\mathbf{P}$ are allocated in $\mathbf{S}$ according to $\mathbf{S} = [P[N_{null}+S_f], P[N_{null}+2S_f], \ldots, P[N-1-N_{null}]]$. A period of $S_f = 6$ data tones per pilot tone is considered in this work.

Each OFDM symbol is extended with a cyclic prefix (CP) before parallel-to-serial conversion. CP lengths of 0%, 6.25%, and 12.5% of the OFDM sizes are considered in this work. When an OFDM frame (a set of serial OFDM symbols) is mounted, a preamble of 2.5 times the length of the OFDM symbol is appended to its beginning for time-domain synchronization and fine frequency synchronization at the receiver. After eight times oversampling and pulse shaping by a raised cosine (RC) filter, the resultant digital signal is pre-modulated by an intermediate frequency (IF) of 6.5 GHz and clipped to 40 % of its maximum for peak-to-average power reduction (PAPR), before being delivered for digital-to-analog conversion (DAC).

B. Experimental Setup

The setup consists of three stations, as shown in Fig. 3(B) and further expanded into Fig. 4, which in a deployment case would be geographically separated: *Station I)* optical signal generation and modulation followed by optical fiber transmission; *Station II)* optical to radio-frequency (RF) conversion followed by W-band RF transmission; and *Station III)* the receiver station.

Station I): Signal generation consists of an external cavity laser (ECL) at λ = 1550 nm, followed by a Mach-Zehnder modulator (MZM) biased at its minimum transmission point and driven with a sinusoidal at $f_{RF}/2 = 43$ GHz to generate two spectral lines spaced at $f_{RF} = 86$ GHz. The signal is amplified by 22 dB using an erbium doped fiber amplifier (EDFA) with a noise figure (NF) $<$ 6 dB and an arrayed waveguide grating (AWG) separates the two spectral lines, allowing to modulate one with data.

A 64 GSa/s arbitrary waveform generator (AWG) serves as a DAC for the signal produced by the digital transmitter layer, as described in section III-A. After a driving amplifier, the signal at a speed of 8 Gbps drives the second MZM with ca. 90% modulation depth. The digital clipping before DAC ensures the majority of the signal will be in the linear range of the MZM transmission curve for optimum extinction ratio.

Two variable optical attenuators (VOAs) ensure equal power of the two arms and allow control over the output optical power. Fig. 5 shows the spectrum of the generated signal at the output of the coupler. A second EDFA with a 4.3 dB NF amplifies the signal by 20 dB before it is transmitted through 10 km of ITU-T G.652 standard single-mode fiber (SMF).

Station II): After fiber transmission the optical signal is converted to an RF signal by beating the two spectral lines on a photodiode (PD) with a nominal 3 dB bandwidth of 100 GHz and a responsivity of 0.5 A/W. The power incident on the PD is varied between -5.5 dBm and 2.5 dBm through the use of the second VOA for analysis of transmission performance. The generated RF signal is amplified by 10 dB and thus mm-wave signals with powers from -20 dBm to -4 dBm are transmitted over a wireless distance of 58 m through a pair of parabolic antennas with a gain of 48 dBi each.

Station III): At the receiver station the signal is amplified by a low noise amplifier (LNA) providing 25 dB gain before down-conversion to an intermediary frequency with a double balanced electrical mixer. The local oscillator for the mixer is obtained by feeding a passive frequency doubler with a sinusoidal at $f_{LO/2} = 37.5$ GHz. Downmixing yields the 8 GHz-wide signal centered at a frequency of $f_{RF-LO} = 11$ GHz. The received signal is amplified by 16 dB and recorded for bit-error rate (BER) measurements using a digital

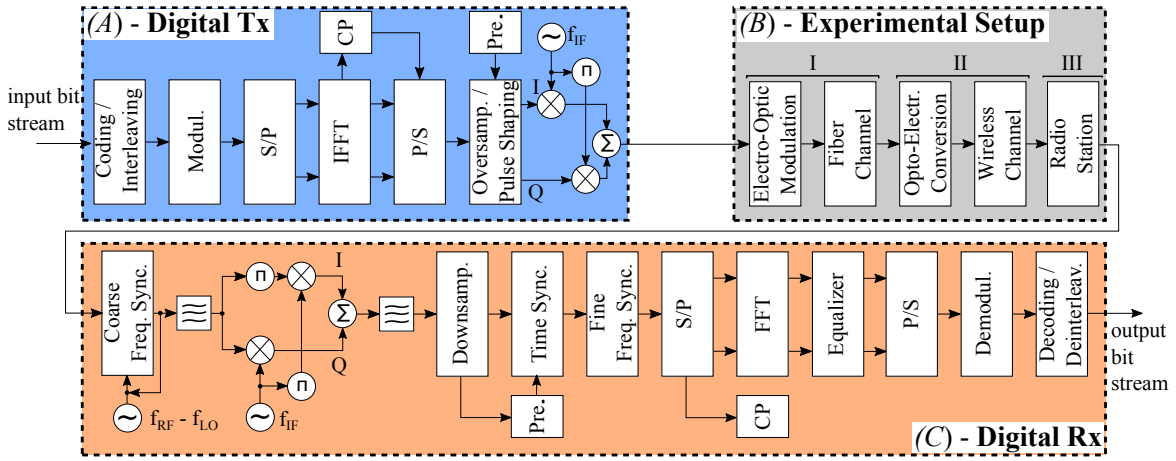

Fig. 3. Block diagram of the proposed system, including digital transmitter (A–top-left), experimental setup (B–top-right), and digital receiver (C–bottom).

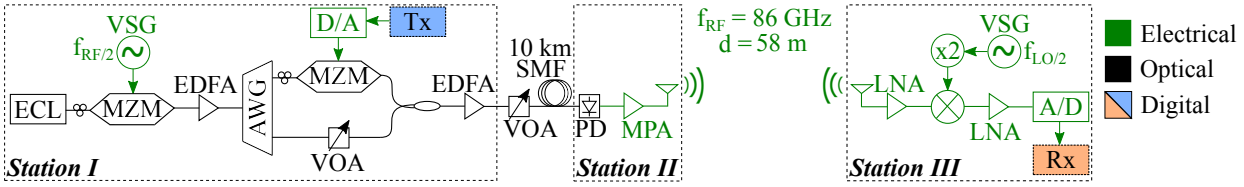

Fig. 4. Schematic of the proposed experimental setup for radio-over-fiber transmission, including optical (black) and electronic components (green). ECL: external cavity laser, VSG: vector signal generator, MZM: Mach-Zehnder modulator, EDFA: erbium doped fiber amplifier, AWG: arrayed waveguide grating, D/A: digital-to-analog conversion (performed by an arbitrary waveform generator - AWG), VOA: variable optical attenuator, SMF: standard single-mode fiber, PD: photodiode, MPA: medium power amplifier, LNA: low noise amplifier, A/D: analog-to-digital conversion (performed by a digital storage oscilloscope - DSO).

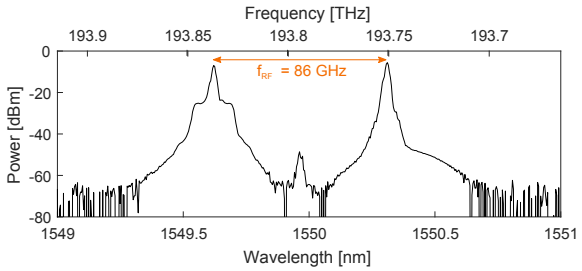

Fig. 5. Signal spectra of the optical signal at the output of the 3 dB coupler, before fiber transmission and photonic upconversion, for the generation of a signal with an 86 GHz carrier.

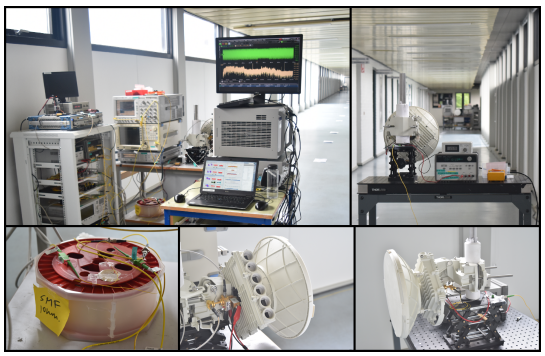

Fig. 6. Experimental Setup. Top-left: *Station I* and *Station III*. Top-right: *Station II*. Bottom-left: fiber span. Bottom-right: transmitting antenna. Bottom-center: receiving antenna.

storage oscilloscope (DSO) that serves as an analog-to-digital converter for further offline digital processing.

A photograph of the laboratory setup is depicted in Fig. 6.

C. Digital Receiver

At the receptor, coarse frequency synchronization and coherent downconversion by $f_{RF} - f_{LO} = 11$ GHz is achieved by a Costas loop. Fig. 7(a) shows the spectrum of the received signal before downconversion. A band pass filter isolates the 8 GHz-wide signal now centred at the intermediate frequency $f_{IF} = 6.5$ GHz, as shown in Fig. 7(b). The resultant digital signal is then demodulated with a 6.5 GHz carrier frequency, as shown in Fig. 7(c), and finally low-pass filtered before being downsampled by a factor of eight, as shown in Fig. 7(d). Fig. 7(d) also shows the baseband original signal spectrum before transmission.

In baseband domain, the appended preamble is used for time synchronization and fine frequency offset correction [23]. After proper CP removal, the process of Fast Fourier Transform (FFT) with size N on the received signal produces the frequency domain symbols as $\tilde{\mathbf{S}} = \mathcal{F}(\mathbf{R})$. The received pilot tones $\tilde{\mathbf{P}}$ are extracted from $\tilde{\mathbf{S}}$ at their positions in the sub-carrier domain. Then, the least-square (LS) algorithm estimates the channel effects $\hat{H}[k]'_{LS}$ as:

$$\hat{H}'_{LS}[m] = \frac{\tilde{P}[m]}{P[m]}, \quad m = 0, 1, \ldots, \left\lceil \frac{N_U}{S_f} \right\rceil - 1, \qquad (5)$$

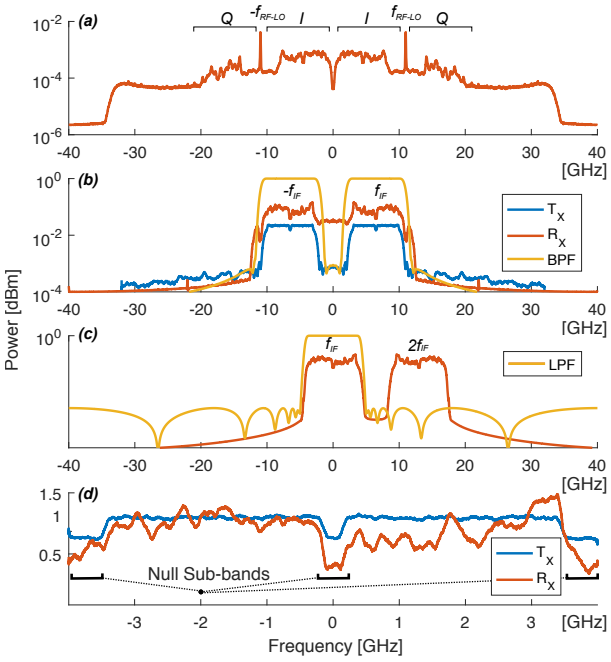

Fig. 7. Signal spectra of the signal and the digital filters: (a) after analog-to-digital conversion, and before RF-LO carrier recovery, (b) T_X signal before IF modulation (in blue), and R_X signal before IF post-demodulation (in red), (c) R_X signal before downsampling, (d) baseband T_X and R_X signals.

where N_U is the number of used sub-carriers and S_f stands for the period of pilot tones in the sub-carrier domain, as explained in section III-A. Subsequently, $\hat{\mathbf{H}}'_{LS}$ is interpolated by *zero-padding* and *low pass filtering* to generate $\hat{\mathbf{H}}_{LS}$, which can be written for each subcarrier as $\hat{H}_{LS}[k]$, $k = 0, 1, \ldots, N-1$. The channel estimate $\hat{\mathbf{H}}_{LS}$ (as illustrated in Fig. 8) is utilized to generate an estimation of the transmitted data symbols as $\hat{\mathbf{S}} = \tilde{\mathbf{S}}/\hat{\mathbf{H}}_{LS}$.

Although the LS channel estimation does not consider the loss of orthogonality between sub-carriers, it has been widely used for channel estimation due to its simplicity. However, its mean-square error (MSE) is inversely proportional to the signal-to-noise ratio (SNR), which implies that it may be subject to noise enhancement, especially when the channel is in a deep null [8]. The wavelet symbols are then extracted from their positions, deinterleaved and finally decoded according to Eq. (3) for BER evaluation.

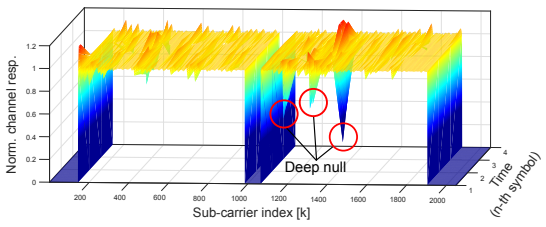

Fig. 8. Estimated baseband channel response, obtained as described in Eq. (5), for a 2048-sized OFDM symbol.

IV. Results and Discussion

A. Experimental Results

Recent simulation based studies [20] for the performance of WC-OFDM systems on slow-varying frequency selective channels indicated that coding gains of nearly 4 dB to 6 dB are achieved in relation to convolution-coded OFDM systems for a BER of 1e-3. In this work, the performance of WC-OFDM communication systems is experimentally evaluated on a composite radio-over-fiber link with 10 km optical transmission through standard SMF plus 58 m wireless transmission in the W-Band. Results were obtained for transmitted signals with a fixed rate of 1 pilot tone for every 6 data tones, within a bandwidth of 8 GHz on a radio frequency of 86 GHz, where each transmission is recorded 25 times, resulting in a total of 924.000 analyzed bits. Three OFDM resolutions, three CP lengths and two pilot levels were considered. Table I summarizes how these values affect the the number of used sub-bands per OFDM symbol (N_U), the sub-band spacing (ΔB), the number of OFDM symbols per OFDM frame (N_{symb}), the preamble transmission time (τ_{pre}), the transmission time of each OFDM symbol (τ_{symb}), the total frame transmission time (τ_{total}), the net bitrate (R), and the spectral efficiency (SE) on the use of the channel.

Fig. 9 shows the results obtained in terms of BER vs. optical power for 2×128 WC-OFDM signals with different FFT sizes and CP lengths. As can be seen, better BER is observed insofar as the OFDM resolution (FFT size) decreases. This effect is explained by the fact that the larger the OFDM resolution is, the longer the OFDM symbols duration (τ_{symb}) gets – as shown in Table I – implying a larger phase walk off between the RF signal after the PD and the LO at the receiver, thus strongly affecting the transmission coherence

TABLE I
Transmission parameters for a baseband oversampling factor of eight times, to a sampling rate of 64 GSa/s

			FFT Size		
			512	1024	2048
		N_U	420	840	1680
		ΔB (MHz)	15.62	7.81	3.90
		N_{symb}	22	10	4
		τ_{pre} (ns)	160	320	640
GI Size	0 %	τ_{symb} (ns)	64	128	256
GI Size	6.25 %	τ_{symb} (ns)	68	136	272
GI Size	12.5 %	τ_{symb} (ns)	72	144	288
GI Size	0 %	τ_{total} (μs)	1.568	1.600	1.664
GI Size	6.25 %	τ_{total} (μs)	1.656	1.680	1.728
GI Size	12.5 %	τ_{total} (μs)	1.744	1.760	1.792
GI Size	0 %	R (Gbps)	4.910	4.375	3.365
GI Size	6.25 %	R (Gbps)	4.649	4.166	3.240
GI Size	12.5 %	R (Gbps)	4.415	3.977	3.125
GI Size	0 %	SE (bit/s/Hz)	0.6138	0.5469	0.4206
GI Size	6.25 %	SE (bit/s/Hz)	0.5811	0.5208	0.4050
GI Size	12.5 %	SE (bit/s/Hz)	0.5519	0.4971	0.3906

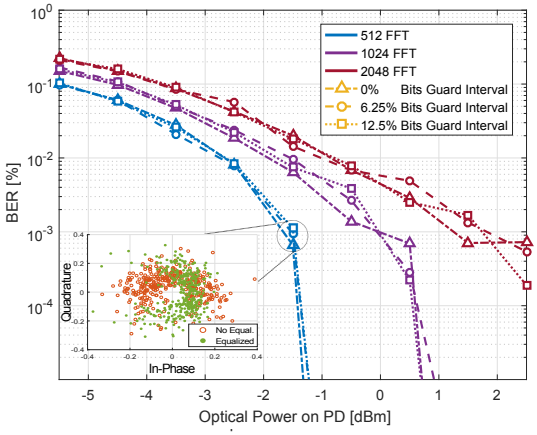

Fig. 9. BER vs. Optical Power on PD for WC-OFDM signals with different FFT sizes and CP lengths. Dark-blue curves represent the performance of 512-sized OFDM. Purple curves represent the performance of 1024-sized OFDM. Dark-red curves represent the performance of 2048-sized OFDM. Triangle marks (△) represent the situation in which 0 bits is used as CP, circle marks (◯) represent the situation in which 6.25% bits of the FFT size are used as CP, Square marks (□) represent the situation in which 12.5% bits of the FFT size are used as CP. The bottom-left constellation represents space of 11-PSK signals for 2×128 WC-symbols before and after equalization.

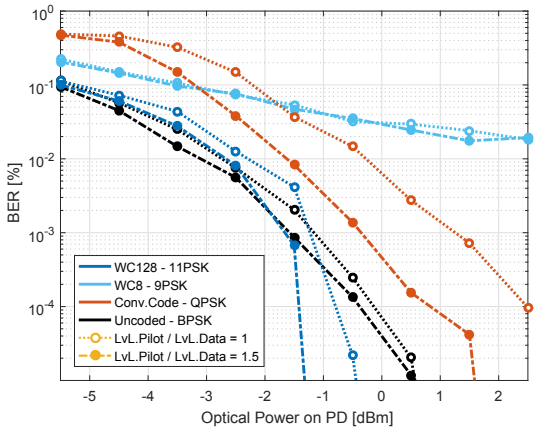

Fig. 10. BER vs. Optical Power on PD for different transmission schemes of equivalent spectral efficiency of 1 bit/s/Hz. Dark-blue curves represent the performance of WC-OFDM transmission with 2×128 Coding Wavelet Matrix and 11-PSK modulation. Light-blue curves represent the performance of WC-OFDM transmission with 2×8 Coding Wavelet Matrix and 9-PSK modulation. Red curves represent the performance of Convolution Code with rate 1/2 and QPSK modulation. Black curves represent the performance of uncoded BPSK scheme. Pointed lines with unfilled circles (· ○ ·) represent the situation in which pilot tones have the same level as data tones, whereas dashed lines with filled circles (-●-) represent the situation in which pilot tones have 1.5 times more power than data tones.

due to degradation of sub-band orthogonality. Moreover, it can be seen that, regardless of the OFDM resolution, an increase of the CP length does not yield any performance improvement. This is striking evidence that the propagated signal was not subjected to any significant multipath propagation, as was expected since greatly directive antennas were used for a single-input-single-output (SISO) line-of-sight (LoS) wireless transmission, and because no multipath phenomena are expected from transmission within SMF.

Fig. 10 shows the results obtained in terms of BER vs. optical power incident on the PD for four transmission schemes with equivalent spectral efficiency of 1 bit/s/Hz, two ratios of pilot-tone level over data-tone level, and a fixed OFDM resolution of 512 sub-bands per symbol. The first thing to notice is that a greater pilot/data level ratio resulted in better performance, regardless of the coding scheme—with the exception of the 2×8 WC case. This effect is a consequence of improved equalization although at the price of decreased SNR, showing a trade-off where finding an optimum configuration yields large performance gains. It should be stressed however, that due to power limitations imposed by some of the utilized electronic components—such as A/D and D/A converters, mixers etc.—it was expected that a further increase in the pilot/data level ratio would not lead to any greater performance improvement.

For a fixed BER of 1e-4, Fig. 10 shows the 2×128 WC scheme with a pilot/data level ratio of 1.5 to outperform the uncoded BPSK scheme by 1 dB. Furthermore, the 2×128 WC outperforms the convolutional QPSK scheme by nearly 2.5 dB.

B. Discussion

From prior studies on WC [17], it is expected that, in purely additive white Gaussian noise (AWGN) channels, both the 2×8 and the 2×128 WC schemes have the same performance as the uncoded BPSK scheme. It is moreover expected, still assuming a purely AWGN channel, that the convolutional coded scheme should outperform the uncoded scheme, even considering a twice higher-dimension signal constellation – which does not occur. These evidences point to the conclusion that the observed propagation channel is indeed subject to some frequency selectivity, as observed in Fig. 8, even in such a purely LoS SISO link with the 1st Fresnel zone within a radius of 22 cm.[1] A detailed investigation on the frequency response of the wireless W-Band channel and previous findings [4], [5] corroborate this conclusion.

Moreover, as chromatic dispersion (CD) will not significantly affect an 8 GHz signal within an optical link of 10 km of SMF, nor is the channel affected by multipath (as concluded from Fig. 9), there is a substantial indication that such a frequency selectivity is caused by the composite non-flat frequency response of electronic and optical components within the setup. While component bandwidths at all stages were larger than that of the signal – the MZM and driver amplifier have a BW of 40 GHz, the RF amplifiers are full band W-Band and the IF amplifier has a BW of ca. 25 GHz – their frequency response within the their bandwidth may vary and especially for the RF amplifiers will not be flat. Combined with non-flat frequency response of the antennae and most significantly that of the mixer employed for down-conversion these may cause the distortions observed in Fig. 7 and Fig. 8.

The observed results suggest that the diversity gains provided by WC do compensate for fading effects in digital transmission, corroborating results from previous studies [18]–[20]. The reduced performance of the 2×8 WC scheme indicates that, due to the trade-off between diversity gain

[1] $r = 17.32 \times \sqrt{0.058[Km]/(4 \times 86[GHz])} = 0.22\ m$

and SNR reduction resulting from the more complex signal constellation, the use of this particular coding-modulation dimension is not recommended for the proposed scenario. However, the performance improvements observed from the use of a larger-dimension WCM are very consistent with results obtained in prior studies [17] inasmuch as greater diversity gains can compensate for more frequent deep fading caused by the channel. The potential gains enabled by WC thus make it a strong candidate for additional coding in future mobile communications.

V. Conclusions

Several methods have been presented to compensate unsolved frequency selectivity in OFDM systems, including the application of channel coding over the sub-carrier domain. These solutions usually require either an expensive computational complexity or some decrease in system spectral efficiency. Confirming the findings of [19] and [20], that WC can substantially compensate for the combined effects of deep frequency fading and error bursts disrupting orthogonality among OFDM sub-carriers, we experimentally demonstrate transmission of 4.9 Gbps 2×8 and 2×128 WC-OFDM signals over a radio-over-fiber link of 10 km fiber plus 58 m wireless distance (with distances of 100 m and beyond predicted to be achievable analog to [5]), using a radio carrier frequency of 86 GHz. We find that, for a fixed BER of 1e-4, the 2×128 WC scheme outperforms an uncoded BPSK by 1 dB while outperforming a convolutional coded QPSK by nearly 2.5 dB.

Considering a SISO LoS setup, the results indicate that the proposed system is able to compensate for the combined effects of noise bursts and frequency distortions caused by electronic components. It is important to stress that these results confirm the theory of Tzannes [16] that the WC enables high diversity gains with a low complexity receiver, without compromising the system's spectral efficiency. Moreover, the results also validate the solution proposed in [18] on modulation schemes that support the integration of WC with power-limited systems. To the best of the authors' knowledge, this is the first time that the transmission of WC signals has been experimentally demonstrated.

The current study indicates that the proposed system fits as a key enabler for the use of mm-wave frequencies in future generation mobile communications, due to its robustness to the harsh effects of frequency selective channels caused either by unsolved multipath or, as in the case of this work, by the highly non-flat frequency response of the employed RF and optical components. It is worth noting though that the Wavelet-Coding algorithm presented in this work is still tied up to 1 bit/s/Hz modulation schemes. Future work should therefore consider strategies to allow higher order modulation formats. Moreover, further investigation must be done on the effects of frequency offset, time offset, and phase distortions on the performance of the proposed system. Signal fading between the antennas should also be considered.

References

[1] L. Kazovsky, S. W. Wong, T. Ayhan, K. M. Albeyoglu, M. R. Ribeiro, A. Shastri, "Hybrid Optical-Wireless Access Networks", *Proceedings of the IEEE*, vol. 100, no. 5, pp. 1197-1225, May 2012.

[2] T. S. Rappaport, S. Sun, R. Mayzus, H. Zhao, Y. Azar, K. Wang, G. N. Wong, J. K. Schulz, M. Samimi, F. Gutierrez, "Millimeter Wave Mobile Communications for 5G Cellular: It Will Work!", *IEEE Access*, pp. 335-349, May 2013.

[3] L. Cavalcante, S. Rommel, J. J. Vegas Olmos, I. T. Monroy, "On the capacity of radio-over-fiber links at the W-band", *Springer Optical and Quantum Electronics*, vol. 48, no. 5, pp. 1-10, Apr 2016.

[4] S. Rommel, L. Cavalcante, A. G. Quintero, A. K. Mishra, J. J. Vegas Olmos, I. T. Monroy, "W-band photonic-wireless link with a Schottky diode envelope detector and bend insensitive fiber", *OSA Optics Express*, vol. 24, no. 11, pp. 11312-11322, May 2016.

[5] S. Rommel, S. Rodriguez, L. Chorchos, E. P. Grakhova, A. K. Sultanov, J. P. Turkiewicz, J. J. Vegas Olmos, I. T. Monroy, "Outdoor W-Band Hybrid Photonic Wireless Link Based on an Optical SFP+ Module", *IEEE Photonics Technology Letters*, vol. 28, no. 21, pp. 2303-2306, Nov 2016.

[6] B. Sklar, "Rayleigh Fading Channels in Mobile Digital Communication Systems Part I: Characterization", *IEEE Communications Magazine*, vol. 35, no. 7, pp. 90-100, Jul 1997.

[7] W. Gao, C. Duan, J. Zhang, "Subcarrier Spreading for ICI Mitigation in OFDM/OFDMA Systems", *IEEE Conferece on Communications*, pp. 1-6, May 2010.

[8] Y. S. Cho, J. Kim, W. Y. Yang, C. G. Kang. *MIMO-OFDM Wireless Communications with MATLAB*, Chichester, UK, John Wiley & Sons, Ltd., 2010.

[9] T. Masakawa, H. Ochiai, "Design of Reed-Solomon Codes for OFDM Systems with Clipping and Filtering", *IEEE Wireless Communications and Networking Conference*, pp. 1361-1366, Mar 2007.

[10] M. Chen, X. Xiao, J. Yu, F. Li, Z. R. Huang, H. Zhou, "Demonstration of Software-Reconfigurable Real-Time FEC-Enabled 4/16/64-QAM-OFDM Signal Transmission in an X-Band RoF System", *IEEE Photonics Journal*, vol. 8, no. 2, Apr 2016.

[11] W. Jian, C. Liu, H.-C. Chien, S.-H. Fan, "Link performance improved 16QAM-OFDM 60-GHz Radio-over-Fiber system employing convolutional codes", *IEEE Optical Fiber Communication, collocated National Fiber Optic Engineers Conference*, p. OThO4, Mar 2010.

[12] A. Vallavaraj, G. S. Brian, K. H. David, G. M. Francis, "Optimizing the Rate 1/2 Convolutional Code for OFDM Applications in terms of Bit-Error-Rate and Peak-to-Average Power Ratio", *IEEE GCC Conference*, pp. 1-6, Mar 2006.

[13] B. Lu, X. Wang, "A Space-Time Trellis Code Design Method for OFDM Systems", *Springer Wireless Personal Communications*, vol 24, no. 3, pp.403-418, Feb 2003.

[14] Z. Cao, J. Yu, Q. Tang, G. Zeng, L. Chen, "Long-reach 60-GHz radio-over-fiber system based on turbo-coded OFDM", *OSA Chinese Optics Letters*, vol. 8, no. 11, pp. 1024-1027, Nov 2010.

[15] I. B. Djordjevic, L. Xu, T. Wang, "Adaptive LDPC-coded OFDM for radio-over-fiber technologies", *IEEE LEOS Annual Meeting Conference Proceedings*, pp. 448-449, Oct 2009.

[16] M. A. Tzannes, "Bit-by-bit Channel Coding Using Wavelets", *Proceedings of IEEE GLOBECOM*, vol. 2, pp. 684-688, Dec 1992.

[17] L. F. Silveira, "Análise da Codificação Wavelet em Sistemas Sujeitos ao Desvanecimento Rayleigh Plano", Ph.D. dissertation, Dept. Electrical Engineering, Universidade Federal do Rio Grande do Norte, Natal, RN, Brazil, 2006.

[18] L. F. Silveira, L. G. Silveira, F. M. Assis, E. L. Pinto, "Analysis and Optimization of Wavlet-Coded Communication Systems", *IEEE Transactions on Wireless Communications*, vol. 8, no. 2, pp. 563-567, Feb 2009.

[19] L. Cavalcante, L. F. Silveira, S. Rommel, J. J. Vegas Olmos, I. T. Monroy, "Performance Analysis of Wavelet Channel Coding in COST207-based Channel Models on Simulated Radio-over-Fiber Systems at the W-Band", *Springer Optical and Quantum Electronics*, vol. 48, no. 1, pp. 1-9, Jan 2016.

[20] L. Cavalcante, R. Dinis, L. G. Silveira, L. F. Silveira, J. J. Vegas Olmos, I. T.Monroy, "Wavelet-Coded OFDM for Next Generation Mobile Communications", *IEEE Vehicular Technology Conference*, In press, Sep 2016.

[21] H. Resnikoff, R. Wells, *Wavelet Analysis: The Scalable Structure of Information*, New-York, USA, Springer-verlag, 1998.

[22] A. Gorokhov, J. P. Linnartz, "Robust OFDM Receivers for Dispersive Time–Varying Channels: Equalization and Channel Acquisition", *IEEE Transactions on Communications*, vol. 52, no. 4, pp. 572-583, Apr 2004.

[23] H. Minn, V. K. Bhargava, K. B. Letaief, "A Robust Timing and Frequency Synchronization for OFDM Systems", *IEEE Transactions on Wireless Communications*, vol. 2, no. 4, pp. 822-839, Jul 2003.